Identification of *FGFR4*-activating mutations in human rhabdomyosarcomas that promote metastasis in xenotransplanted models

James G. Taylor VI,[1] Adam T. Cheuk,[2] Patricia S. Tsang,[2] Joon-Yong Chung,[3] Young K. Song,[2] Krupa Desai,[1] Yanlin Yu,[4] Qing-Rong Chen,[2,5] Kushal Shah,[1] Victoria Youngblood,[1] Jun Fang,[6] Su Young Kim,[7] Choh Yeung,[7] Lee J. Helman,[7] Arnulfo Mendoza,[8] Vu Ngo,[9] Louis M. Staudt,[9] Jun S. Wei,[2] Chand Khanna,[8] Daniel Catchpoole,[10] Stephen J. Qualman,[11] Stephen M. Hewitt,[3] Glenn Merlino,[4] Stephen J. Chanock,[6] and Javed Khan[2]

[1]Pulmonary and Vascular Medicine Branch, National Heart, Lung, and Blood Institute (NHLBI), NIH, Bethesda, Maryland, USA. [2]Oncogenomics Section, Pediatric Oncology Branch, [3]Tissue Array Research Program, Laboratory of Pathology, and [4]Cancer Modeling Section, Laboratory of Cancer Biology and Genetics, Center for Cancer Research (CCR), National Cancer Institute (NCI), NIH, Bethesda, Maryland, USA. [5]Advanced Biomedical Computing Center, SAIC-Frederick Inc., NCI-Frederick, Frederick, Maryland, USA. [6]Laboratory of Translational Genomics, Division of Cancer Epidemiology and Genetics, NCI, NIH, Bethesda, Maryland, USA. [7]Molecular Oncology Section, Pediatric Oncology Branch, [8]Tumor and Metastasis Biology Section, Pediatric Oncology Branch, and [9]Metabolism Branch, CCR, NCI, NIH, Bethesda, Maryland, USA. [10]Oncology Research Unit, Children's Hospital at Westmead, Westmead, New South Wales, Australia. [11]Center for Childhood Cancer and Children's Research Institute, Nationwide Children's Hospital, Columbus, Ohio, USA.

Rhabdomyosarcoma (RMS) is a childhood cancer originating from skeletal muscle, and patient survival is poor in the presence of metastatic disease. Few determinants that regulate metastasis development have been identified. The receptor tyrosine kinase *FGFR4* is highly expressed in RMS tissue, suggesting a role in tumorigenesis, although its functional importance has not been defined. Here, we report the identification of mutations in *FGFR4* in human RMS tumors that lead to its activation and present evidence that it functions as an oncogene in RMS. Higher *FGFR4* expression in RMS tumors was associated with advanced-stage cancer and poor survival, while *FGFR4* knockdown in a human RMS cell line reduced tumor growth and experimental lung metastases when the cells were transplanted into mice. Moreover, 6 *FGFR4* tyrosine kinase domain mutations were found among 7 of 94 (7.5%) primary human RMS tumors. The mutants K535 and E550 increased autophosphorylation, Stat3 signaling, tumor proliferation, and metastatic potential when expressed in a murine RMS cell line. These mutants also transformed NIH 3T3 cells and led to an enhanced metastatic phenotype. Finally, murine RMS cell lines expressing the K535 and E550 *FGFR4* mutants were substantially more susceptible to apoptosis in the presence of a pharmacologic FGFR inhibitor than the control cell lines expressing the empty vector or wild-type *FGFR4*. Together, our results demonstrate that mutationally activated *FGFR4* acts as an oncogene, and these are what we believe to be the first known mutations in a receptor tyrosine kinase in RMS. These findings support the potential therapeutic targeting of FGFR4 in RMS.

Introduction

Rhabdomyosarcoma (RMS) is a pediatric sarcoma arising from skeletal muscle, with which the majority of patients can be subclassified as having either alveolar RMS (ARMS) or embryonal RMS (ERMS). ARMS is observed in older patients and is associated with a chromosomal translocation creating a fusion gene involving *FOXO1A* on chromosome 13 and members of the *PAX* gene family. ERMS is characterized by loss of heterozygosity and altered patterns of genomic imprinting (1). Despite marked improvement in overall prognosis during the last 4 decades, long-term survival for those with metastatic RMS remains poor (<30%) (2). Factors contributing to tumor progression and metastatic disease are not well understood.

Analysis of RMS gene expression patterns have led to improved diagnostic accuracy and new insights into possible mechanisms for metastatic regulators including SIX1 and EZRIN (3–5). We and others have reported that FGF receptor 4 (*FGFR4*), a receptor tyrosine kinase (RTK) member of the *FGFR* gene family, is highly expressed in RMS and that its mRNA expression correlates with protein levels (3, 4, 6). FGFR4 is also a key regulator of myogenic differentiation and muscle regeneration after injury, although it is not expressed in differentiated skeletal muscle (7–9). These observations raise the possibility that FGFR4 is not only a tumor-specific marker, but that it could also function as an oncogene in RMS.

The FGFRs are of considerable interest in cancer biology because they regulate essential processes including cellular survival, motility, development, and angiogenesis (10). Comparison of the complete FGFR coding regions indicates segments of high amino acid conservation in FGFR1, -2, -3, and -4. Germline mutations in these paralogs have been described for several rare Mendelian skeletal disorders, including hypochondroplasia (11, 12). RTKs may also be activated in human cancer by point mutations such as the somatic mutations within FGFR tyrosine kinase (TK) domains observed

Authorship note: J.G. Taylor VI and Adam T. Cheuk contributed equally to this work.

Conflict of interest: J. Khan, A.T. Cheuk, and J.G. Taylor VI are named as inventors with the NIH on a provisional patent application for the therapeutic treatment of cancers overexpressing *FGFR4* or harboring *FGFR4* mutations.

Citation for this article: *J. Clin. Invest.* **119**:3395–3407 (2009). doi:10.1172/JCI39703.

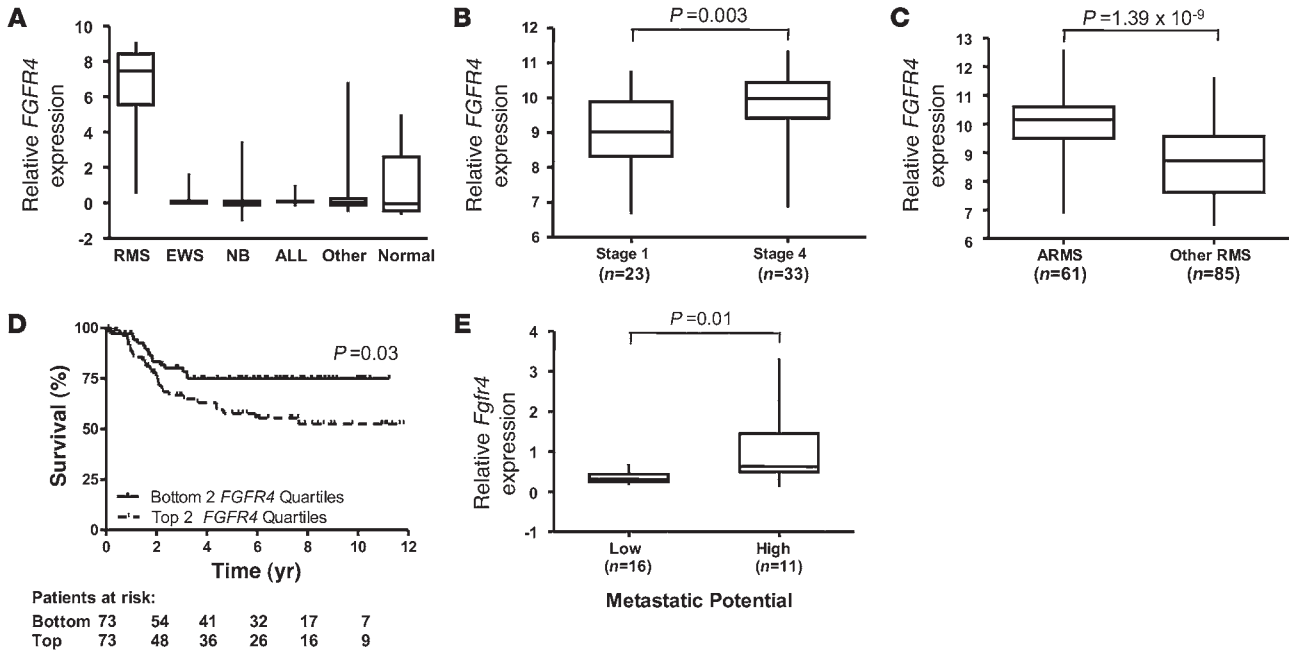

Figure 1

High *FGFR4* expression in RMS is associated with advanced stage, ARMS histology, and poor survival. (**A**) Log_2 median-centered expression data showed high *FGFR4* expression in RMS tumors compared with other pediatric tumors and normal tissue of human tumors. EWS, Ewings sarcoma; NB, neuroblastoma; ALL, acute lymphoblastic leukemia; other, other pediatric tumors; normal, normal tissue. (**B**) Stage 4 RMS was associated with significantly higher median *FGFR4* expression than stage 1 RMS, as analyzed based on the data of Davicioni et al. (Mann-Whitney test) (6). (**C**) *FGFR4* expression was significantly higher in ARMS compared with all other histologic RMS subtypes (Mann-Whitney test). (**D**) Kaplan-Meier analysis based on a cutoff of median *FGFR4* expression showed that patients with higher expression (top 2 quartiles) had significantly higher mortality (than the bottom 2 quartiles; $P = 0.03$, log-rank test). (**E**) Murine RMS cell lines (derived from refs. 5, 21) of high metastatic potential had significantly higher median *Fgfr4* mRNA than nonmetastatic cell lines ($P = 0.01$, Mann-Whitney test).

in glioblastoma multiforme, endometrial carcinoma, and lung cancer (13–17). However, *FGFR4* is infrequently mutated in these and other cancers (13, 18, 19). It has also been reported that an aberrant FGFR4 isoform promotes tumorigenesis in pituitary adenomas, although the mechanism for the expression of this transcript was not due to somatic mutation but thought to be due to regulation by an alternative promoter (20). Since *FGFR4* is highly expressed in RMS and during myogenesis, but not in mature skeletal muscle, we hypothesized that constitutive FGFR4 activation by either overexpression or mutation would promote an aggressive phenotype in RMS.

Results

FGFR4 expression in RMS shows correlation with FGFR4 protein, advanced stage, ARMS histology, and poor survival. Since we previously demonstrated high *FGFR4* expression in RMS tumors (3), we first investigated whether its expression was associated with aggressive clinical behavior, using available RMS expression microarray data sets (3, 5, 6). We confirmed high *FGFR4* expression in primary RMS tumors compared with an independent panel of pediatric tumors and normal tissues (Figure 1A). Consistent with prior observations, mRNA overexpression was associated with high FGFR4 protein (Supplemental Figure 1; supplemental material available online with this article; doi:10.1172/JCI39703DS1) (3). Analysis of an RMS data set for which clinical follow-up was available showed that *FGFR4* messenger RNA was 2-fold higher in stage 4 metastatic tumors compared with stage 1 ($P = 0.003$), although there was some overlap in the range of expression between the 2 groups (Figure 1B) (6). ARMS also had higher expression compared with non-ARMS tumors (Figure 1C; $P = 1.39 \times 10^{-9}$). Kaplan-Meier analysis for different FGFR4 expression quartiles showed a significant trend toward lower survival with higher expression (Supplemental Figure 2) and significantly lower overall survival for tumors with higher *FGFR4* expression (Figure 1D; $P = 0.03$) (6). Further univariate analysis of this data set confirmed that high stage and ARMS histology were also associated with lower survival (Table 1). However a Cox proportional hazards multivariate analysis revealed that only clinical stage was associated with early death (Table 1; hazard ratio = 9.17; $P = 0.002$), indicating a strong association of *FGFR4* expression with clinical stage and ARMS histology. To further validate the association of increased expression with advanced-stage disease, we also reexamined gene expression data from cell lines derived from a spontaneous model of murine ERMS (5, 21) and found significantly higher *Fgfr4* expression in tumors of high metastatic potential (Figure 1E; $P = 0.01$).

Because DNA amplification or gain can lead to increased mRNA expression levels, we next examined *FGFR4* DNA copy number for a set of 94 RMS tumors and measured the mRNA levels for those samples with increased copy number variation (> 2.5, $n = 15$). We could not demonstrate a correlation between high copy number variation and mRNA expression of *FGFR4* ($r^2 = 0.0127$, P = NS; Supplemental Table 1). This suggested that high *FGFR4* expression was not due to amplification at the genomic level.

Table 1
Sub-analyses of *FGFR4* expression on survival in RMS

Analysis parameter	Hazard ratio	95% Confidence interval	*P*
Univariate			
Stage (3/4 vs. 1/2)	6.30	2.25–17.67	0.0005
Histology (ARMS vs. others)	2.87	1.44–5.72	0.003
FGFR4 expression (high vs. low)	1.97	1.08–3.48	0.03
Multivariate			
Stage (3/4 vs. 1/2)	9.17	2.19–38.39	0.002
Histology	2.29	0.96–5.46	0.06
FGFR4 expression	0.94	0.43–2.45	0.94

FGFR4 suppression inhibits RMS tumor growth and lung metastasis. To characterize the role of *FGFR4* expression in the promotion of RMS tumor progression and metastasis, we stably introduced an inducible shRNA directed against *FGFR4* into the human ARMS cell line RH30. Induction of this shRNA decreased FGFR4 protein expression by nearly 92% (Figure 2A) but did not result in reduced in vitro growth for up to 4 days in tissue culture (Figure 2B). However, there was a 41% reduction ($P = 0.002$) in growth after prolonged culture for 13 days (Figure 2C). We then proceeded to study the phenotypic consequences of reduced FGFR4 expression in vivo. FGFR4 suppression resulted in significantly smaller tumors 31 days after intramuscular injection into SCID Beige mice compared with controls (Figure 3, A and B; $P = 0.002$). Quantification of early arrest of metastatic cells in the lungs 24 hours after injection by intravital video microscopy (IVVM) revealed significantly fewer RH30 cells with FGFR4 suppression (Figure 3, C and D; $P = 0.008$). A comparable reduction in IVVM early lung metastases was also observed in the highly metastatic murine RMS cell line RMS33 with *Fgfr4* suppression (Supplemental Figure 3; $P = 0.02$) (5). Of note, there were also fewer pulmonary metastases with FGFR4 suppression 74 days after intravenous injection of inducible RH30 cells (Figure 3E). To confirm that this difference was not due to a reduced growth rate of the cells, we normalized for the growth rate by calculating the ratio of pulmonary to pelvic tumor signals and found a significant reduction upon FGFR4 suppression (Figure 3F; $P = 0.02$).

Identification of FGFR4 TK domain mutations in human RMS tumors. Our results thus far indicated that increased *FGFR4* activity could contribute to tumor progression and metastatic disease in RMS. Therefore, we searched for activating *FGFR4* mutations using bidirectional sequencing of all protein coding exons and their intron/exon borders in the same 94 RMS tumors (Supplemental Table 2). We found 14 missense variants, of which 6 were clustered in the TK domain (Figure 4A). Four of the TK domain mutations were localized to codons 535 and 550 (Table 2; Figure 4, A–C; and Supplemental Figure 4). None of these TK missense substitutions were present in the Human Gene Mutation database, COSMIC, or a large sequencing survey of RTK genes (18). A subset of these tumors (50 of 94) had paired germline DNA available. For these, 3 of 3 TK domain mutations were found only in the tumors and not in germline DNA and were therefore somatic (Supplemental Table 2). We did not observe mutations in the *FGFR4* TK domain in 9 human RMS cell lines.

We confirmed that these TK domain mutations were absent in healthy populations by additional bidirectional sequencing of the 2 *FGFR4* exons corresponding to codons 507 to 607 in 1,030 multiethnic controls (Supplemental Table 2). These findings suggested an overall TK domain mutation prevalence of 7.5% (7 of 94 tumors; 95% confidence interval, 4.7%–10.2%; Table 2) versus only a single R529Q single nucleotide variant allele observed among the 1,030 healthy controls (0.1%; $P = 2.0 \times 10^{-7}$ for tumors vs. controls).

Predictive analysis of FGFR4 mutations. To determine the significance of these mutations, we performed multiple predictive analyses for individual amino acid substitutions (see Methods and Supplemental Table 3). These suggested that the 4 *FGFR4* missense substitutions at codons 535 and 550 were most likely to result in disruption of protein function (Supplemental Table 3) (22–26). Furthermore, the codon 535 and 550 mutations mapped to adjacent sites within the hinge region on a model of the FGFR4 TK domain (Figure 5A). Codon 535 mutations are predicted to eliminate the FGFR4 R-group hydrogen bonds that inhibit receptor autophosphorylation or regulate conformational dynamics during phosphorylation in the paralog FGFR2 (Figure 5, B–D) (27, 28), while those at codon 550 are predicted to alter the ATP binding cleft (29, 30).

Mutations promote FGFR4 autophosphorylation, Stat3 phosphorylation, and activation of cell cycle and DNA replication pathways. We functionally characterized 2 of these 4 TK domain mutations (K535 and E550) to determine whether they would result in constitutive

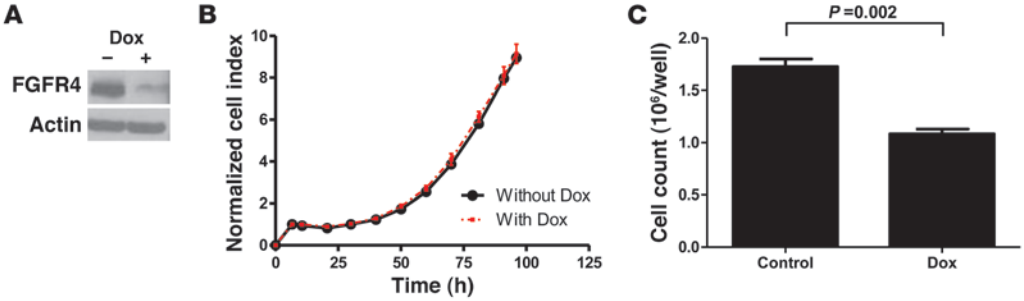

Figure 2
FGFR4 knockdown with an inducible shRNA leads to reduced in vitro growth. (**A**) Western blot confirmed suppression of FGFR4 with doxycycline induction of the shRNA in RH30 cells. (**B**) Growth curves for RH30 cell lines with an inducible shRNA directed against *FGFR4* showed no measurable difference in growth rate for up to 96 hours. (**C**) Cell count of RH30 cell lines with an inducible shRNA against FGFR4 treated with or without doxycycline shows significantly reduced growth (41% reduction) with prolonged culture at 13 days (Mann-Whitney test).

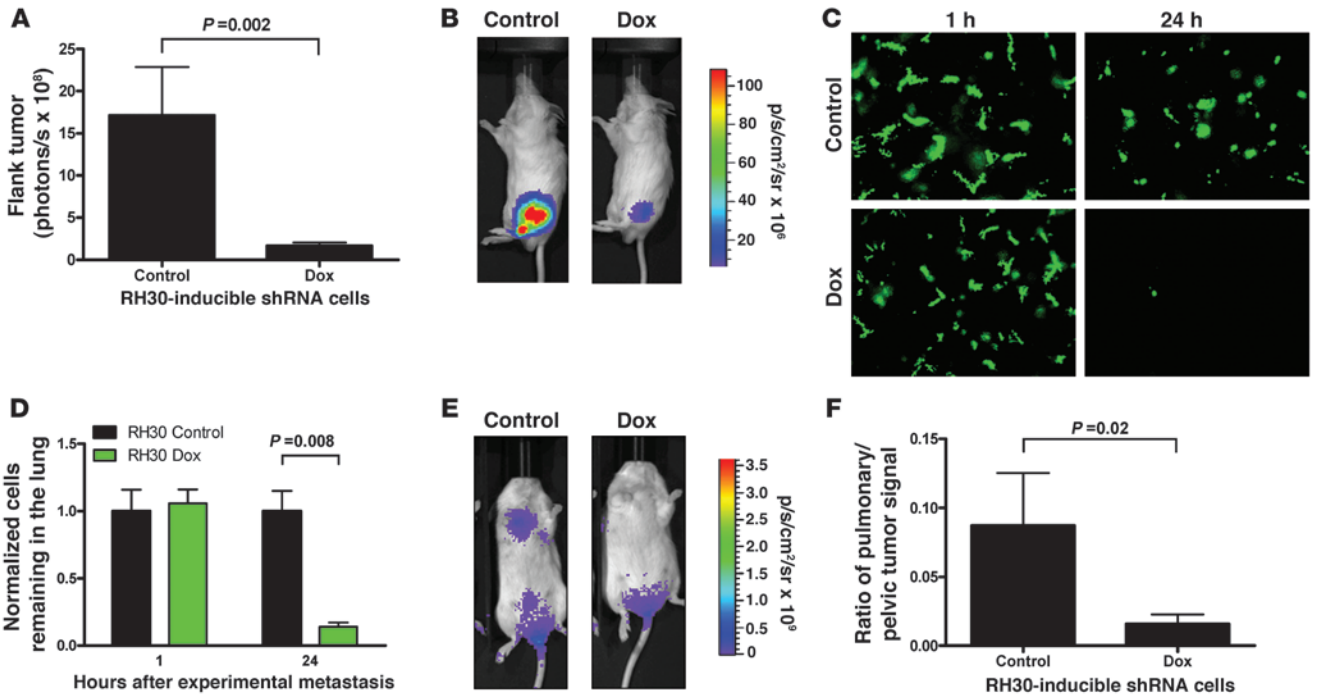

Figure 3

FGFR4 suppression leads to inhibition of in vivo growth and lung metastasis. (**A**) Intramuscular injection of RH30 with inducible anti-*FGFR4* shRNA resulted in significantly smaller tumors in the FGFR4-suppressed mice on day 31 using bioluminescent imaging (n = 6 mice per group, Mann-Whitney test). (**B**) Representative mice with intramuscular injection on day 31. The intensity of tumor cells expressing luciferase is quantified as photons/second/cm^2/steridian (p/s/cm^2/sr). (**C**) Representative IVVM images showing decreased RH30 cells in the lungs at 24 hours when FGFR4 was suppressed. (**D**) Quantification of IVVM early pulmonary metastases at 1 and 24 hours showed significantly fewer malignant cells remaining in the lungs with FGFR4 suppression (normalized mean values ± SEM; n = 5 mice per group; Mann-Whitney test). (**E**) Representative mice with intravenous injection showed decreased tumor signal in the lungs with FGFR4 suppression on day 74. (**F**) Intravenous injection of the same cells resulted in significantly fewer lesions in the lungs on day 74 in the FGFR4-suppressed mice (normalized for tumor growth rate by taking the ratio of pulmonary to pelvic tumor signal; n = 10 mice per group, Mann-Whitney test).

receptor activation. We transduced wild-type human *FGFR4* or mutants K535 and E550 into the murine RMS cell line RMS772, which was previously derived from a spontaneous tumor occurring in a mouse model of ERMS (5, 21). RMS772 was chosen because of its low metastatic potential and undetectable *Fgfr4* mRNA (5). We confirmed expression of *FGFR4* in transduced cell lines at both RNA and protein levels, with FGFR4 protein levels that were comparable with 2 human RMS cell lines (Figure 6, A and B). Of note, both of these mutations resulted in significant FGFR4 receptor autophosphorylation (Figure 6C).

Western blot analysis of known FGFR downstream signaling molecules found significant differences in the Stat, Akt, and Mapk/Erk pathways with increased total Stat3 and phospho-Stat3 in both mutant lines (Figure 6D). Interestingly, the mutant cell lines also had a decrease in phospho-Akt and a discernible difference in the Mapk pathway with decreased phospho-Erk1/2 in both wild-type *FGFR4* and mutant transductants compared with the vector control (Figure 6D). Other signaling molecules including mTor, S6k, 4Ebp1, and Gsk3β showed no significant differences between transductants (Supplemental Figure 5).

We then examined the global downstream effects of expressing these human mutations in RMS772 cells using gene expression profiling. Gene set enrichment analysis showed that the mutants had significant upregulation of cell cycle and DNA replication gene pathways (false discovery rate [FDR] < 0.01), while cell adhesion pathways and markers of muscle differentiation were diminished (Table 3 and Figure 6E).

FGFR4 mutants increase proliferation, invasion, and metastatic potential. The association of high *FGFR4* expression with advanced stage and poor survival and the upregulation of cell cycle genes led us to hypothesize that constitutive *FGFR4* activation would be associated with increased growth and result in a metastatic phenotype in RMS. Both the K535 and E550 mutations caused significantly higher growth rates in RMS772 cell lines grown in vitro when compared with wild-type *FGFR4* at 72 hours (Figure 7A; P = 0.0071 and 0.0090, respectively). Consistent with these data, subcutaneous injection of the RMS772 transductants into nude mice demonstrated rapid increases in tumor volume for the mutants at 18 days (Figure 7B; both P = 0.0079), providing evidence for increased in vivo growth.

Using a modified Boyden chamber invasion assay, we found 3-fold enhanced invasiveness associated with *FGFR4* mutant cell lines compared with the vector control or wild-type *FGFR4* in RMS772 (Figure 7C; P = 0.002 for vector versus K535; P = 0.005 for E550). Cellular arrest in the lungs and early metastasis was assayed by IVVM in mice after intravenous injection of fluorescently labeled RMS772 transductants. IVVM at 1 hour after injection demonstrated an equal number of cells for all 4 transductants. However, only the mutations significantly enhanced the presence of foci in

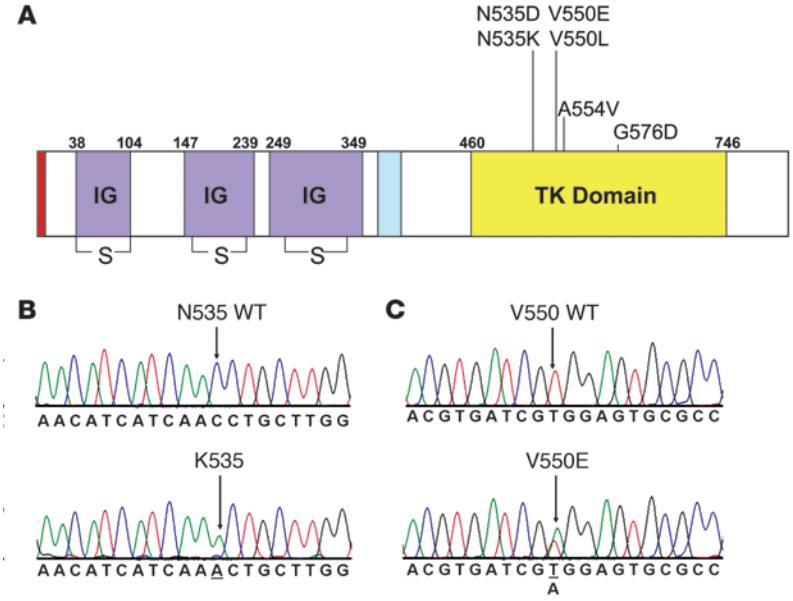

Figure 4
FGFR4 TK domain mutations in RMS. (**A**) Sites of 6 missense substitutions in the FGFR4 TK domain that were identified in RMS tumors (n = 94). Amino acid boundaries for protein domains were defined by the results of a search of the NCBI Conserved Domain database (NCBI CD-Search). Red, signal peptide; blue, transmembrane domain. IG, immunoglobulin-like domain; S, disulfide bond. (**B**) Wild-type and homozygous mutant alleles for the N535K mutation. (**C**) Wild-type and mutant alleles for V550E.

the lungs after 24 hours (46-fold and 22-fold increase for K535 and E550, respectively, compared with vector control), although there was a small (2.6-fold) but significant increase in the number of foci caused by the wild-type human FGFR4 (Figure 7D). To determine whether these differences in growth and invasion influence in vivo metastatic potential, RMS772 cells expressing wild-type human *FGFR4* or mutations were introduced into nude mice intravenously. At 3 weeks, mutant cell lines produced significantly more gross pulmonary metastases compared with those expressing wild-type *FGFR4* (Figure 7E). In a follow-up experiment, Kaplan-Meier survival analysis demonstrated earlier mortality for mice injected with mutant cell lines (Figure 7F; $P < 0.0001$ by log-rank test for trend; median survival: E550, 19 days; K535, 29 days; wild type, 59 days; vector control, 78 days). Necroscopy confirmed large tumor burden in the lungs due to metastatic disease (Figure 7F).

To validate these results in an independent cell line, we transduced NIH 3T3 cells with the same constructs and repeated the in vivo subcutaneous growth and intravenous experimental metastasis assays. We again observed rapid growth in mice receiving subcutaneous NIH 3T3 cells transduced with *FGFR4* K535 or E550, compared with no growth among the controls at 18 days (Figure 8A). Intravenous injection of 3T3 cell lines similarly resulted in earlier mortality due to metastatic disease in animals receiving mutant *FGFR4* cells (Figure 8B; $P < 0.0001$ by log-rank test for trend).

Effect of mutations on cell cycle, apoptosis, and FGFR inhibition. Our results predicted mutational activation of an oncogenic pathway. Consequently, we tested whether these mutations would result in increased survival under adverse conditions and whether RMS tumor cells become dependent upon *FGFR4* activation for survival, potentially making them more sensitive to a FGFR inhibitor. Despite the increased proliferation rate of mutant cell lines grown in 10% serum (Figure 7A), there were no differences in the distribution in the cell cycle compared to the empty vector or wild-type *FGFR4* (Figure 9A). However, both vector and wild-type controls had significantly higher proportions of apoptotic cells under conditions of serum starvation compared with mutant cell lines, as demonstrated by an increased subG1 fraction (Figure 9B).

To demonstrate oncogene dependence upon mutational activation of FGFR4, the 4 cell lines were treated with the FGFR inhibitor PD173074 (29, 31). We confirmed that PD173074 treatment

Table 2
FGFR4 TK domain mutations observed in primary RMSs

Case ID	FGFR4 codon	Nucleotide	Genotype[A]	Mutation type	Histology	Pax-FKHR fusion[B]	Stage[C]
6	N535	Ch5:176455020	N/D	—[D]	ERMS	Absent	Unknown[E]
13	N535	Ch5:176455022	K/K	—[D]	Unknown[F]	Absent	Unknown[E]
18	N535	Ch5:176455020	N/D	—[D]	Unknown[F]	Absent	Unknown[E]
36	V550	Ch5:176455157	V/L	—[D]	ARMS	PAX3-FKHR	Unknown[E]
64	V550	Ch5:176455158	V/E	—[D]	ERMS	Absent	III
231	V550	Ch5:176455157	V/L	Somatic	ERMS	Absent	III
248	A554	Ch5:176455170	V/V	Somatic	ARMS	PAX3-FKHR	I
	G576	Ch5:176455236	D/D	Somatic			

[A]Predicted diploid amino acid genotype at each codon. [B]Both Pax3-FKHR and Pax7-FKHR fusion transcripts were assayed by RT-PCR. [C]According to the Intergroup Rhabdomyosarcoma Study Group pretreatment staging classification (2). [D]Paired germline DNA was not available. [E]Clinical stage information was not available. [F]Histological RMS subtypes were not available.

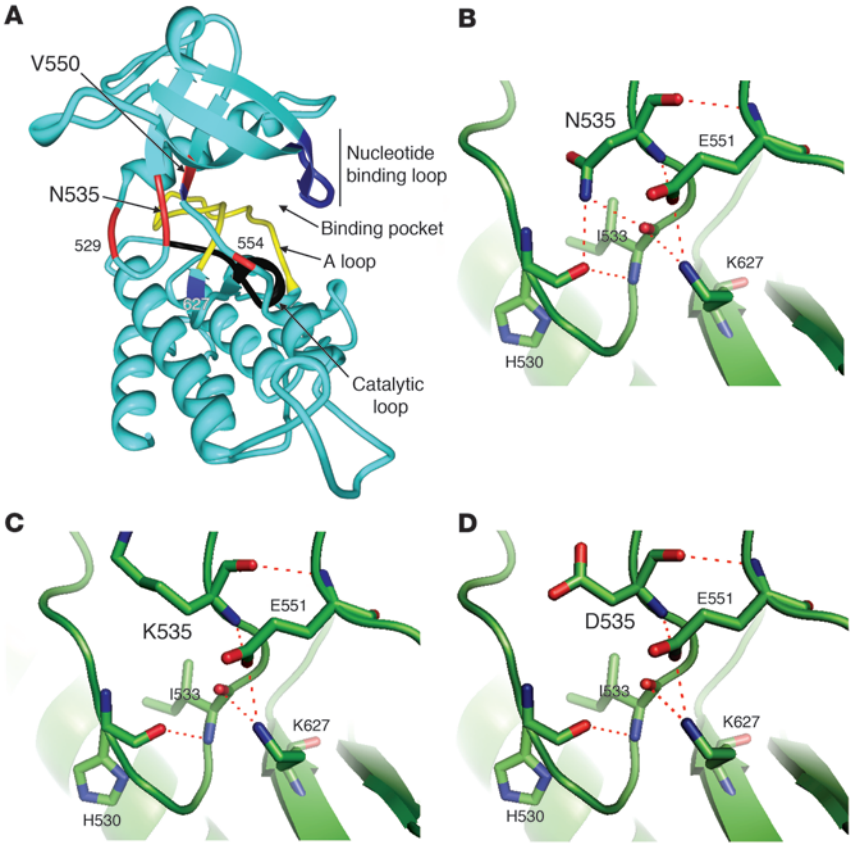

Figure 5
Structural modeling of the *FGFR4* codon 535 and 550 mutations. (**A**) Codon 535 and 550 mutations (red) on a model of the FGFR4 kinase domain. Mutation sites of codons 529 and 554 are also in red. The activation loop (A loop) is yellow, the catalytic loop black, and the nucleotide binding loop blue. (**B**) Predicted hydrogen bonds for wild-type codon 535. (**C** and **D**) Codon 535 mutations could disrupt R-group hydrogen bonds (red dashed lines) between codon 535 and residues H530 and I533. Illustrations in **B**–**D** were created with PyMOL (http://www.pymol.org).

reduced phospho-FGFR4 (normalized to total FGFR4) for both K535 and E550 mutants (Figure 9C). The IC_{50} after 48 hours of treatment decreased from 12.7 μM and 11.8 μM in the vector control and wild-type *FGFR4* cell lines to 8.2 μM and 5.9 μM for K535 and E550, respectively (Figure 9D). Increased apoptosis with PD173074 was apparent in both mutant cell lines, as evidenced by an increased SubG1 fraction (Figure 9E) and increased activated caspase-3 (Figure 9F).

Discussion

RMS is an aggressive childhood cancer arising from skeletal muscle precursors. While significant progress has been made in the overall survival of patients treated for RMS, metastatic disease remains a considerable challenge, with less than 30% survival despite aggressive multimodal therapies (2). Therefore, there is a critical need for the development of targeted therapeutics in patients presenting with advanced-stage RMS.

We and others have previously reported *FGFR4* mRNA and protein overexpression in RMS (3, 4, 6), although none of these studies elucidated its functional importance in RMS pathogenesis or its potential as a molecular target for therapy. *FGFR4* is also expressed in myoblasts during normal development, in regenerating muscle following injury, but not in mature skeletal muscle (6–8, 32). PAX3 and PAX7 directly induce *FGFR4* expression, resulting in the progression of embryonic progenitor cells into a myogenic program (7). Furthermore, PAX3/7-FOXO1A chimeric transcription factors are present in the majority of ARMS (33), and they increase the expression of target genes more than wild-type PAX3 or PAX7 (34). This predicts that these chimeric fusion products, produced as a result of chromosomal translocations, could be strong inducers of *FGFR4* in ARMS.

These reports suggest that FGFR4 pathway activation may result in a rhabdomyoblast phenotype by enhancing proliferation and blocking terminal differentiation in RMS. Therefore, we hypothesized that FGFR4 activation may be oncogenic in RMS and represent a potential novel therapeutic target. Here, we demonstrate that high *FGFR4* expression was significantly associated with protein levels, ARMS histology, metastatic disease, and poor survival. However, in a multivariable regression analysis, *FGFR4* mRNA expression was not independent of high stage or ARMS histology, since both of these parameters are associated with poorer prognosis and high *FGFR4* expression (35). This association would also be expected if *FGFR4* is a direct target of the PAX3/7-FOXO1A fusion transcription factors. Moreover, we found that suppression of wild-type FGFR4 resulted in a significant reduction in local growth and fewer early and late pulmonary metastases in xenograft models.

Oncogene activation has been described to occur through overexpression, gene amplification, or mutation (36–39). Our results suggested that overexpression might result in increased activity and led us to hypothesize that activating *FGFR4* mutations might also be present in RMS (5, 6). In this study we confirmed *FGFR4* TK domain–activating mutations in 7.5% of RMS tumors, which were not present in normal populations. Additionally, all of the *FGFR4* TK domain mutations were somatic in the subset of the RMS patients that had tumor DNA mutations and a paired germline DNA sample. This does not rule out the existence of germline *FGFR4* mutations in addition to somatic mutations if larger populations or pedigrees were to be surveyed. However, given the domi-

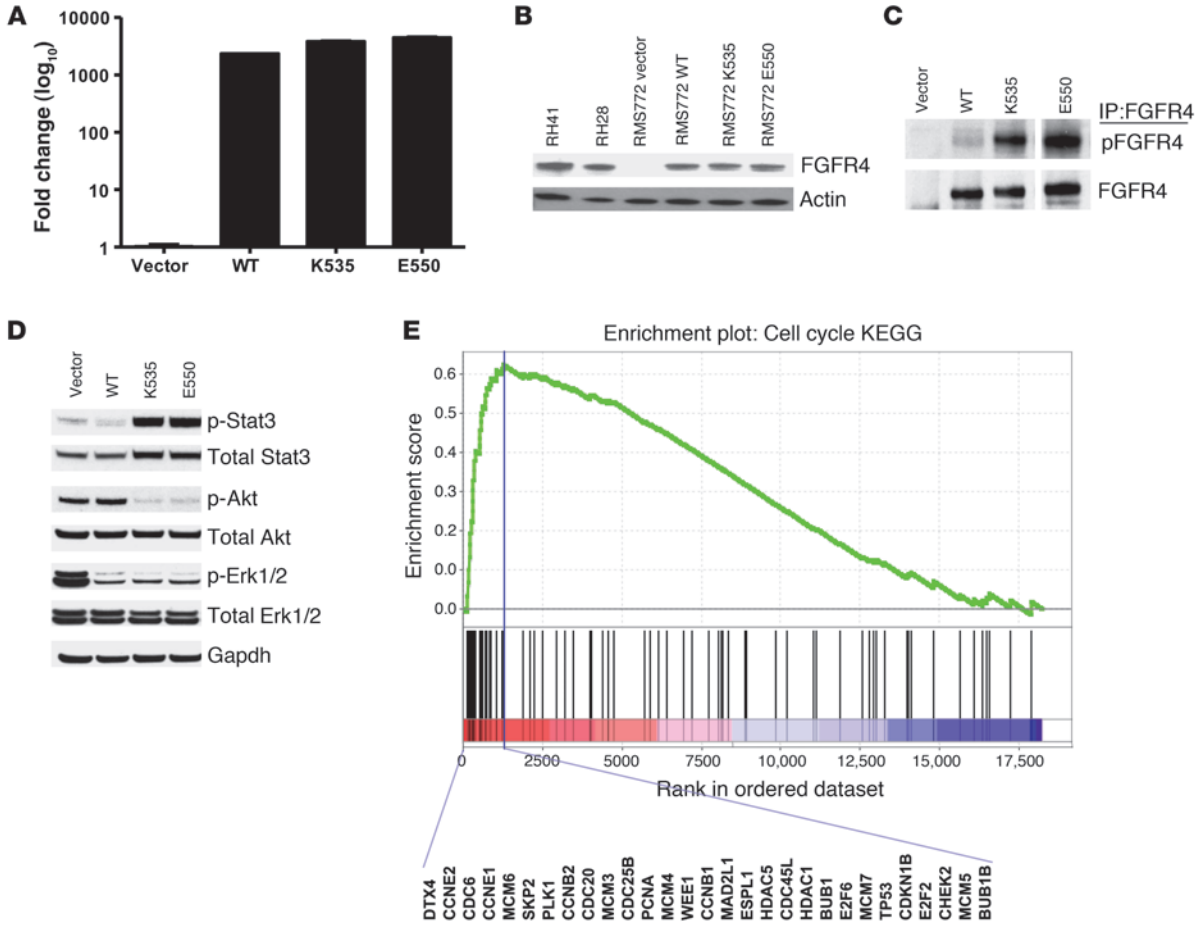

Figure 6

FGFR4 mutations promote FGFR4 autophosphorylation, STAT3 phosphorylation, and activation of cell cycle and DNA replication pathways. (**A** and **B**) High levels of RNA (**A**) and protein (**B**) for wild-type human *FGFR4*, *FGFR4* K535, and *FGFR4* E550 after stable introduction into murine RMS cell line RMS772. Protein levels are comparable to those of human RMS cell lines RH41 and RH28. (**C**) Immunoblot of FGFR4 and phospho-FGFR4 after immunoprecipitation showed that the mutant forms of FGFR4 were constitutively autophosphorylated. (**D**) Increased total Stat3 and phospho-Stat3 were observed in FGFR4 mutant cell lines by immunoblot, while mutants also showed decreased phospho-Akt. All transductants expressing human FGFR4 also had less phospho-Erk1/2. (**E**) Representative GSEA showing enrichment of cell cycle genes in murine RMS cells expressing *FGFR4* mutations. Gene names listed at the bottom are at the leading edge of genes ranked by expression enrichment score that also belong to the Cell Cycle KEGG gene set.

nant action of these mutations, it seems unlikely that germline mutations of this gene would result in normal development.

Computational analysis of these TK domain mutations predicted that they would likely result in FGFR4 autophosphorylation with resultant downstream pathway activation, as was confirmed by our studies. Notably, a significant increase in Stat3 activation was observed. Stat3 activation has previously been associated with cell growth and survival in RMS and other cancers and is known to occur downstream of the FGFRs (40–43). Of interest, investigation of the Akt pathway revealed that both *FGFR4* mutations suppressed phospho-Akt. This is consistent with previous findings that germline, activating *FGFR2* mutations result in suppression of phospho-AKT and that inactive AKT can promote invasion and metastasis (44–46). We speculate that the phenotypic consequences of FGFR4 mutational activation are mediated by oncogenic and metastatic effects of Stat3. Further work is required to determine which of these cellular alterations dictate the metastatic phenotype.

RTKs that are activated by point mutations have been shown to be drivers of tumorigenesis and represent ideal targets for therapy (36–39, 47). Previously identified RMS mutations that could be exploited therapeutically include PAX3/7-*FOXO1A* gene translocation/fusions found only in ARMS and RAS missense mutations (*NRAS*, *KRAS*, and *HRAS*), reported in a small number of ERMS (33, 48–50). However, targeting fusion transcription factors remains a significant challenge, and the mutations in RAS genes were found in studies in which only a small number of ERMS tumors were surveyed. Importantly, this is the first report of activating RTK mutations that are common to both histological types of RMS.

More generally, our study represents the highest prevalence of *FGFR4* TK domain mutations reported in human cancers, while other large-scale cancer genomic screens have found infrequent missense mutations in *FGFR4* (13, 18, 19, 51–54). Additionally, none of the missense mutations identified in this study were found in adenocarcinoma of the lung, which has the highest prevalence

Table 3
Altered expression of 6 pathways in cells expressing *FGFR4* TK domain mutations by GSEA

Annotated cellular function	Overlapped genes	Genes in the leading edge	Source[A]	FDR
Upregulated in mutants K535 and E550				
Cell cycle Kegg	79	29	GenMAPP	<0.01
Cell cycle	72	27	GO	<0.01
DNA replication reactome	39	17	GenMAPP	<0.01
Downregulated in mutants K535 and E550				
Striated muscle contraction	31	16	GenMAPP	<0.01
Cordero KRAS KD control up	68	23	Broad Institute	<0.01
Cell adhesion	141	30	GO	<0.01

[A]Gene sets from the Broad Institute (Molecular Signatures Database; http://www.broadinstitute.org/gsea/msigdb/index.jsp), GenMAPP (Gene Map Annotator and Pathway Profiler; http://www.genmapp.org), and GO (Gene Ontology; http://www.geneontology.org/).

of *FGFR4* mutations reported to date (1.8%) (13, 51). In addition, 2 of the 4 mutations occurring at codons 535 and 550 are known to be mutated in FGFR paralogs (FGFR1, -2, and -3 and RET) and in FGFR4 for a single hypermutated breast cancer sample (11, 12, 14, 16, 17, 19, 55, 56).

Functionally these *FGFR4* mutations appear to be significantly more potent than wild-type *FGFR4* overexpression in promoting growth and metastasis, and they were necessary for in vivo neoplastic growth in NIH 3T3 fibroblasts. These findings are in agreement with prior work, which has shown that introduction and overexpression of wild-type *FGFR4* does not transform fibroblasts or support FGF-induced growth in BaF3 cells (20, 41, 57). In contrast, FGFR1–FGFR3 are all able to transform different cells through either overexpression alone or overexpression with FGF stimulation (57, 58), suggesting that FGFR4 has unique signaling and biological responses compared with its FGFR paralogs. Most significantly, these mutations increased invasiveness and promoted a metastasis phenotype and poor survival in our murine RMS models. Prior association studies have shown that a common variant in FGFR4, G388R, is associated with tumor progression in the absence of detectable FGFR4 activation and that this may be due to the role of FGFR4 as a tumor suppressor (59–61). However, our observations demonstrate that *FGFR4* mutational activation leads to an oncogenic phenotype, and this is in accord with others who have suggested that *FGFR4* is an oncogene (13, 20).

Our data suggest that FGFR4 is an excellent candidate for targeted therapy in patients with advanced-stage RMS. Furthermore, we show that 7.5% of RMS tumors harbor predicted activating mutations, and we confirm that 2 of these are driver mutations that lead to enhanced sensitivity to a small molecule inhibitor. These results provide a rational basis for therapeutically targeting the FGFR4 pathway in RMS and other cancers. Overall, our findings have direct implications for rapid translation into adjuvant therapies for metastatic RMS, for which long-term prognosis remains poor.

Methods

Samples and cell lines. Ninety-four primary RMS tumors were obtained for genomic DNA extraction from the Cooperative Human Tissue Network (CHTN) and the Children's Hospital at Westmead. Fifty of these primary RMS tumors had matching germline genomic DNA, also obtained from the CHTN. The demographics for the 44 unpaired and 50 paired tumors are presented in Supplemental Table 4. All tumors with an *FGFR4* TK domain mutation were subject to RT-PCR for the presence of known *PAX-FOXO1* fusion genes as previously described, modified by the use of the 3′ *FOXO1* primer, ATGAACTTGCTGTGTAGGGACAG (62). RT-PCR products (*PAX3/FOXO1* = 172 bp and PAX7/ *FOXO1* = 160 bp) were resolved on an Agilent Bioanalyzer 2100 and analyzed with DNA 1000 Lab-on-chip software (Agilent Technologies). Healthy, anonymous controls included 284 Europeans/European Americans, 30 North Africans, 333 Africans/African Americans, 143 individuals from the Middle East, 175 Asians, and 65 Hispanics/Native Americans. Use of anonymous human tissue samples was exempted from Institutional Review Board approval by the Office of Human Subjects Research, NIH. Human RMS cell lines used for DNA sequencing were A673, RD, RH4, RH5, RH28, RH30, RH36, and RH41.

RNA and genomic DNA purification. Up to 70 milligrams of frozen primary tumor was homogenized in 0.7 milliliters Trizol (Invitrogen). Murine tumor cell lines were grown to 80% confluence, washed with PBS, and resuspended in Trizol. RNA was purified with miRNEasy kits (Qiagen). Genfind (Agencourt) was used to purify tumor DNA and genomic DNA from leukocyte preparations paired with individual tumor samples.

DNA sequencing. PCR primers for 17 *FGFR4* protein–coding exons are presented in Supplemental Table 5. Genomic DNA was amplified by PCR using PCR and PCR clean-up (shrimp alkaline phosphatase/exonuclease I) conditions standardized per the SNP500Cancer database (http://snp500cancer.nci.nih.gov) and a uniform annealing temperature of 65°C. Sequencing of amplified DNA using Big Dye Terminator chemistry (ABI) and M13 forward or reverse primers was performed on ABI platforms (models 3100 and 3730) and analyzed with Sequence Analysis 3.7 (ABI) and Sequencher 4.5 software (Gene Codes Corp.). Twenty percent of samples were sequenced in duplicate, and all missense or single mutations were confirmed with replicate PCR/sequencing reactions.

Quantitative RT-PCR. Two micrograms of total RNA was reverse transcribed using 3 micrograms of random Hexamer and Superscript II reverse transcriptase enzyme (Invitrogen) as per manufacturer's instruction. The resulting cDNA was diluted 1:20 in water, and real-time PCR was performed on an ABI 7000 Sequence Detection System (ABI). Assays-on-Demand (ABI) were used for assessing *FGFR4* expression levels (primer Hs00242558_m1), and fold change was determined by normalizing to *GAPDH* (Hs99999905_m1).

Predictive analysis of FGFR4 mutations. Each *FGFR4* missense mutation was computationally analyzed for a predicted effect on protein function using 4 methods. Sorting Intolerant From Tolerant (SIFT; http://sift.jcvi.org/) was used to calculate a SIFT probability score for the likelihood of the mutation to affect protein function (26). Scores of 0.05 or less were predicted to affect protein function, although approximately 20% of positive SIFT scores represent false-positive predictions. Polymorphism phenotyping (PolyPhen; http://coot.embl.de/PolyPhen) was also used, predicting either unknown (insufficient data for a prediction), benign, possibly damaging, or probably damaging mutations based upon characterization of the substitution site, predicted secondary protein structure, or available 3-dimensional protein structures (24, 25). The third method employed the profile model of SNPs3D (http://www.snps3d.org), which is based upon conservation at an amino acid position and the probability of observing a variant at that site within the protein's family of homologs (22, 23). SNPs3D determines a profile score using a support vector

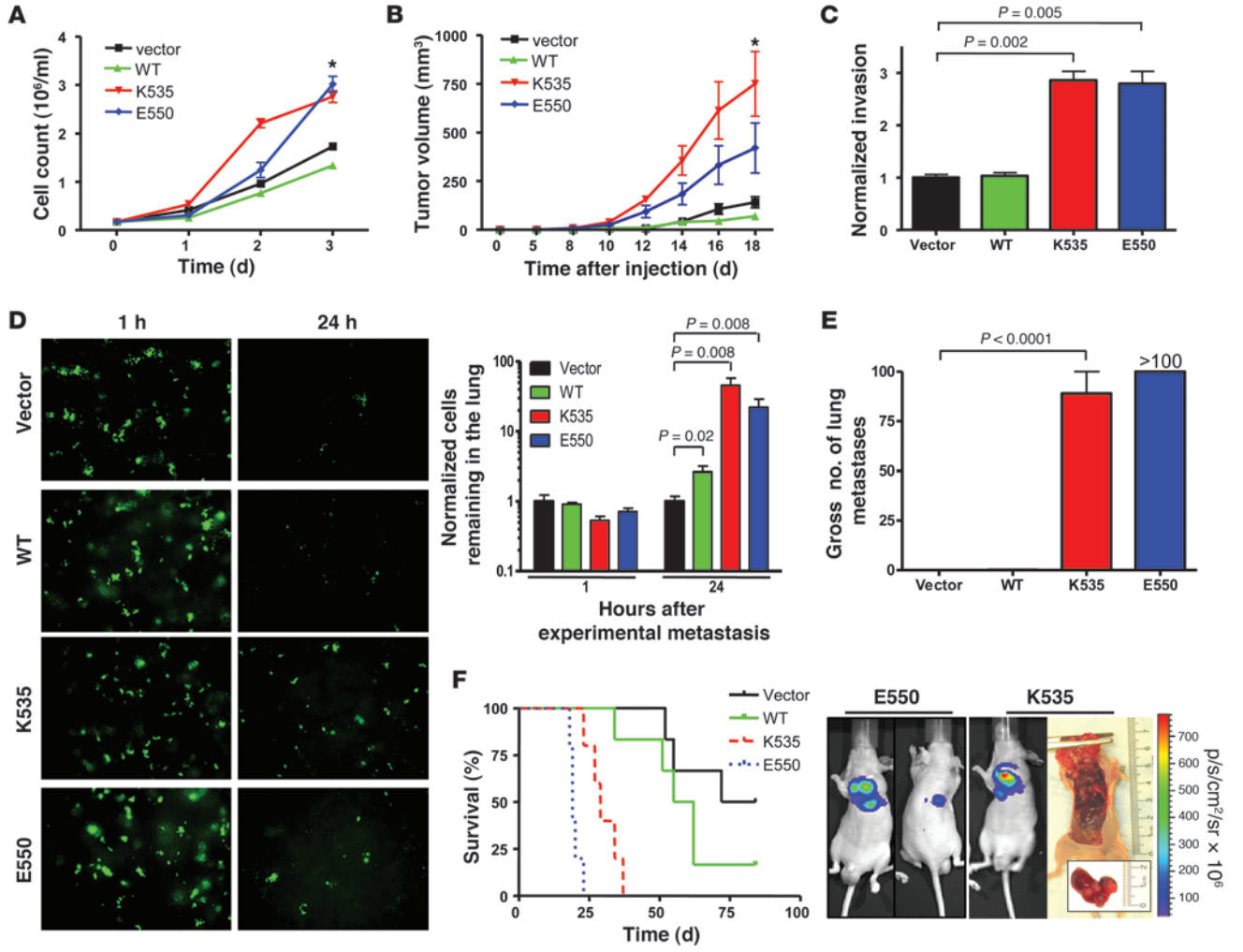

Figure 7

FGFR4 mutations accelerate growth and promote a metastasis phenotype. (**A**) Growth was significantly higher for cultured mutant RMS772 cell lines (*$P < 0.01$ versus wild type, Mann-Whitney test). (**B**) *FGFR4* mutants in RMS772 cells significantly enhanced in vivo growth after subcutaneous injection in nude mice (*$P < 0.001$ versus wild-type, Mann-Whitney test). (**C**) *FGFR4* RMS772 mutants showed 3-fold higher invasion (normalized to the vector control) by a modified Boyden chamber assay (*t* test with Welch correction). (**D**) Left: Representative IVVM images show the presence of RMS cells in the lung (1 and 24 hour time points shown). Right: Quantification of pulmonary lesions at 1 and 24 hours showed the persistence of RMS cells transduced with the 2 mutants (normalized to the vector control at each time point; $n = 5$ mice per group; Mann-Whitney test). (**E**) Gross pulmonary metastases from RMS772 cells at 21 days (comparison using Student's *t* test). (**F**) Left: Kaplan-Meier survival analysis demonstrated a significantly poorer survival in mice injected intravenously with RMS772 cell lines transduced with the 2 mutants. Right: Pulmonary lesions in representative animals injected with mutants are shown.

machine, where negative values are associated with deleterious mutations. Approximately 10% of negative support vector machine scores are predicted to be false positives. Finally, Multivariate Analysis of Protein Polymorphism (MAPP; http://mendel.stanford.edu/SidowLab/) was used to predict the impact of each nonsynonymous variant though a comparative analysis of FGFR4 orthologs and the corresponding physicochemical properties that specific amino acid changes represent (63). Alignment and phylogenetic tree building for 9 FGFR4 orthologs (NP_998812_human, XP_001087243_macaque, XP_518127_chimpanzee, NP_032037_mouse, NP_001103374_rat, XP_414474_chicken, XP_001498550_horse, XP_546211_dog, and SP_602166_cow) was performed using standard procedures for ClustalW2 (http://www.ebi.ac.uk/Tools/clustalw2/index.html) prior to analysis with MAPP. *P* values of less than 0.05 for a particular amino acid substitution represent those mutations likely to impair protein function. Mutations were queried in dbSNP (http://www.ncbi.nlm.nih.gov/SNP), the Human Gene Mutation Database (http://www.hgmd.cf.ac.uk/ac/index.php), and the Catalogue Of Somatic Mutations In Cancer (COSMIC; http://www.sanger.ac.uk/genetics/CGP/cosmic). Amino acid boundaries for FGFR4 protein domains shown in Figure 4 were defined by the results of a search of the NCBI Conserved Domain database (NCBI CD-Search; http://www.ncbi.nlm.nih.gov/structure/cdd/wrpsb.cgi). FGFR4 TK domain structural models (based on NP_998812 and the unphosphorylated FGFR2c TK domain, PDB accession 2psqA) were generated using SWISS-MODEL (http://swissmodel.expasy.org/) and visualized using MBT Protein Workshop (Figure 5A; http://www.rcsb.org) and PyMOL (Figure 5, B–D; http://www.pymol.org).

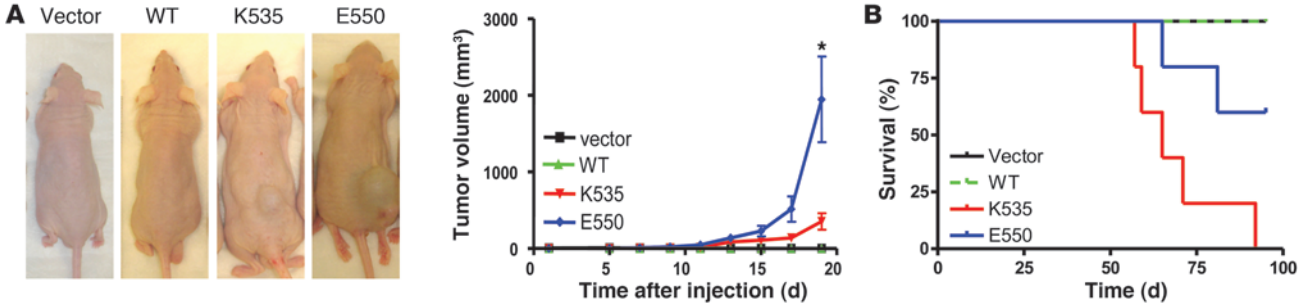

Figure 8

FGFR4 mutations transform 3T3 cells. (**A**) *FGFR4* mutants transformed NIH 3T3 cells and promoted in vivo tumor growth after subcutaneous injection in nude mice (*$P < 0.001$ versus wild type, Mann-Whitney test). Representative animals injected with 3T3 cells transduced with the respective constructs are shown at day 18. In these animals, tumors were observable in 4 of 5 mice (K535) and 5 of 5 mice (E550). (**B**) Kaplan-Meier survival analysis in mice after intravenous injection of NIH 3T3 cells with wild-type and mutant FGFR4 (n = 5 mice per group).

Constructs and cell line transductants. Full-length human *FGFR4* (clone ID 4121396 in pOTB7; Invitrogen) was subcloned into the XhoI site of the pMSCVpuro vector (Clontech Laboratories). Orientation of the gene insert was confirmed by sequencing after the polyA tail was removed. Mutations at either codon K535 or E550 were introduced by site-directed mutagenesis. Wild-type and mutated *FGFR4* clones in pMSCVpuro were confirmed by sequencing. The PT67 cell line (Clontech) was used to package virus, and then cell line RMS772 (5) was transduced with wild-type *FGFR4*, *FGFR4* K535, *FGFR4* E550, or an empty viral vector (control) under puromycin selection. pMSCVzeo retroviral vector expressing firefly luciferase (provided by B. Clary, Duke University Medical Center, Durham, North Carolina, USA) was later transduced into each of these RMS772 cell lines. The RH30 cell line with a transduced tetracycline repressor was transduced with a tetracycline-inducible shRNA (oligo sequence: AGCTAAAAAGCCGTCAAGATGCTCAAAGACTCTCTTGAAGTCTTTGAGCATCTTGACGGCGG) targeting *FGFR4* as described previously (64). The RH30 subclone with the highest *FGFR4* knockdown (clone H11.5) was further transduced with luciferase and then used for all subsequent studies.

Cell culture and in vitro characterization of RMS cell lines. RMS33 and RMS772 cells were cultured in RPMI1640 (Quality Biological Inc.), 2 mM L-glutamine (Quality Biological Inc.) and 1% penicillin/streptomycin (Quality Biological Inc.), and 0%–10% FBS (HyClone). RH30, NIH 3T3, and PT67 cell lines were grown in DMEM (Quality Biological Inc.) supplemented with 10% FBS, 2 mM L-glutamine, and 1% penicillin/streptomycin. For growth characterization, RMS772 was washed with PBS, trypsinized, collected, and then the cells were counted. Invasion assays were performed according to the manufacturer's recommendations in Cultrex 96-well Boyden chambers with 8-micron transmembrane pores, a 0.5X basement membrane extract, and a serum gradient of 0.5% to 1% (Trevigen). Plates were read 24 hours after cell seeding.

In vitro shRNA RH30 cell growth. Real-time cell electronic sensing (ACEA Biosciences Inc.) technology was used to monitor cell growth in a real-time manner. RH30 H11.5 cells (3.0×10^3) were seeded in each well of the 96-well E-plate device. Twenty-four hours after seeding, cells were treated with 25 ng/ml doxycycline. Growth of RH30 H11.5 cells with or without doxycycline was monitored for a total of 96 hours after cells were seeded. Cell count measurements were performed by seeding 1,000 cells into each well of a 6-well plate. Twenty-four hours after seeding, cells were treated with 25 ng/ml doxycycline. Medium was replaced with or without doxycycline every 3 days. The final RH30 H11.5 cell number was measured with or without doxycycline after 13 days.

Immunoblotting. Immunoblotting was performed on cells cultured in 10% FBS and lysed in RIPA buffer supplemented with 1% protease inhibitor (Pierce Biotechnology) and 1% phosphatase inhibitor (Pierce Biotechnology). RH30 H11.5 cells were cultured in the presence or absence of doxycycline (25 ng/ml) for 48 hours prior to immunoblotting. FGFR4 autophosphorylation immunoblots were performed after FGFR4 immunoprecipitation (FGFR4 [C-16] antibody; Santa Cruz Biotechnology Inc.) with protein A/G agarose beads. Twenty micrograms of protein were separated on 4%–12% Bis-Tris gels (Invitrogen) and transferred to nitrocellulose membrane by iBlot (Invitrogen). For FGFR4 phosphorylation immunoblots, membranes were blocked with 5% nonfat dry milk in PBS and 0.1% Tween-20 (PBST) and were probed with antibodies to anti–phospho-tyrosine (clone 4G10; Millipore) and human FGFR4 (C-16; Santa Cruz Biotechnology Inc.). For pathway analyses, membranes were blocked with 5% nonfat dry milk in TBS and 0.1% Tween-20 (TBST) and were probed with the following antibodies (all antibodies from Cell Signaling unless otherwise specified): Akt, phospho-Akt (Ser473), phospho-Gsk3β, phospho-mTor, S6k, phospho-S6k, 4Ebp1, phospho-4Ebp1, Erk1/2, phospho-Erk1/2, Stat3, phospho-Stat3, and Gapdh (Chemicon International). Specific molecules were detected with HRP-conjugated anti-mouse or anti-rabbit secondary antibodies (Pierce Biotechnology/Thermo Fisher Scientific) and enhanced with SuperSignal Chemiluminescence kits (Pierce Biotechnology). Signal was detected on Kodak Biomax MR X-ray film (Kodak).

Cell cycle analysis. BrdU Flow Kits (BD Biosciences — Pharmingen) were used for cell cycle assays. Briefly, cultured cells were grown in the presence or absence of serum or were treated with the FGFR inhibitor PD173074 (CalBiochem) in 10% FBS, pulsed with 1 mM BrdU for 30 minutes, and stained with an anti-BrdU antibody, followed by 7-AAD staining as per the manufacturer's guidelines. FACS was analyzed using CellQuest software (BD Biosciences).

Microarray gene expression analysis. Human *FGFR4* expression from published data sets utilized probe X204579_at from the human U133A GeneChip (Affymetrix). Relative *FGFR4* expression (*Fgfr4* expression, for mice) presented in Figure 1, A–C and E, was calculated by median centering of $\log_2$ expression levels from published microarray datasets (http://home.ccr.cancer.gov/oncology/oncogenomics/ and http://ntddb.abcc.ncifcrf.gov/cgi-bin/nltissue.pl). RMS772 cells for microarray experiments were cultured as described in 0% FBS prior to RNA extraction. Gene expression profiling was performed using mouse genome 430 2.0 Arrays (Affymetrix), and expression data were normalized with DNA Chip Analyzer (dChip) in the PM-only model. The effect of the *FGFR4*

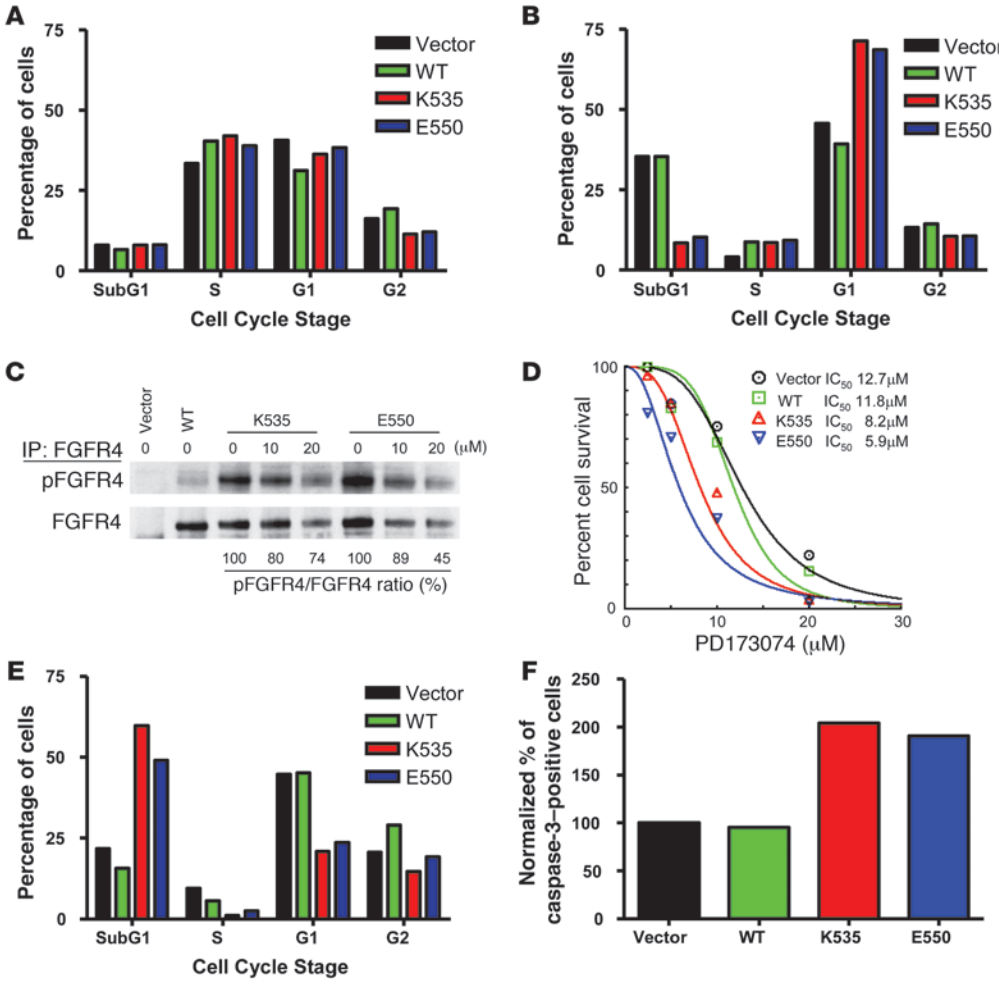

Figure 9
Oncogene dependence and inhibition of *FGFR4*. (**A**) Cell cycle analysis of RMS772 in 10% serum. (**B**) Cell cycle analysis in the absence of serum showed increased apoptotic cells (subG1 fraction) for the vector and wild-type *FGFR4* RMS772 cell lines. (**C**) Inhibition of FGFR4 phosphorylation after PD173074 treatment at 3 hours. (**D**) RMS772 survival after 48 hour treatment with PD173074. IC_{50} values for RMS772 vector control, wild-type FGFR4, K535, and E550 are presented. (**E**) Increased subG1 fraction of mutant RMS772 cells lines after 24 hours of treatment with 20 μM PD173074. (**F**) Increased caspase-3 activation of FGFR4 mutant RMS772 cell lines after 24 hours of treatment with 20 μM PD173074.

mutants on murine RMS cells was determined on the basis of gene set enrichment analysis (GSEA; http://www.broad.mit.edu/gsea), where expression data for K535 and E550 cells were combined and compared to the vector control (65). The gene sets with a FDR of less than 0.01 were considered significant.

In vivo growth, metastasis, and imaging assays. Animal studies using RMS772 and NIH 3T3 constructs utilized 8- to 10-week-old male NU/NU-Fox1^{nu} nude mice (Charles River Laboratories) housed in a pathogen-free environment. Studies with RMS33 and RH30 H11.5 cells used 8- to 10-week-old CB17.B6-Prkdc^{scid} Lyst^{bg}/Crl (SCID Beige) mice (Charles River Laboratories), including those receiving either a normal or a doxycycline diet (Harlan Teklad). Animal care and experimental procedures were approved by the NIH Animal Care and Use Committee. In vivo tumor growth was assessed using RMS772 transductants or NIH 3T3 transductants with 10^6 cells (0.1 milliliters) subcutaneously injected into the flank of each mouse. Mice were monitored every other day, and tumor dimensions were measured by caliper. Tumor volume was determined by the following formula: (long axis × short axis^2) / 2. For RH30 H11.5 experiments, 3×10^6 cells (after 48 hours in 25 ng/ml doxycycline) were injected intramuscularly into SCID Beige mice. Doxycyline diet was initiated 48 hours prior to injection in the treatment group for all RH30 H11.5 experiments, and this diet was continued for the duration of the experiment. Tumor volume was assessed by luciferase photon flux with a Xenogen IVIS 100 imaging system. For FGFR4 knockdown assays, SCID Beige mice were intravenously injected with 10^6 RH30 H11.5 cells per day for 4 consecutive days (after 48 hours in 25 ng/ml doxycycline). Mice were treated with a control or doxycycline diet, and pulmonary metastases were detected with Xenogen imaging. For the other experimental metastasis assays and survival analyses, 10^6 RMS772 cells or 10^5 NIH 3T3 cells, either expressing or not expressing luciferase, were intravenously injected into tail veins of nude mice as previously described (5). Cells fluorescently labeled with CMFDA (Invitrogen) were assayed for early metastasis by IVVM as previously described at 1 and 24 hours after tail vein injection (66). Gross tumor number in lung tissue was assessed by observation at necroscopy (day 21) for an end-point metastasis assay. For survival analysis, mice were imaged twice weekly with a Xenogen IVIS 100 imaging system until the protocol end point, when the mice appeared weak and sick.

In vitro response to treatment with PD173074. The protein TK inhibitor PD173074 was purchased from CalBiochem and resuspended in DMSO. RMS772 transduced cell lines were seeded in 96-well plates overnight in full culture medium and 10% serum as described above. The inhibitor was added at various concentrations ranging from 0 μM to 20 μM. Cell number was determined separately at 24-hour intervals with Cell Titer Glo (Promega). Caspase-3 activity was determined using PE Active Caspase-3 Apoptosis kits (BD Biosciences — Pharmingen).

Statistics. Statistical analysis was performed using Instat and Prism 4 (both from Graph Pad Software). Continuous data were compared with

P values by paired *t* test or Mann-Whitney *U* test, as appropriate. Survival was analyzed by Kaplan-Meier curve comparison using a log-rank test and with a multivariate Cox proportional hazards analysis. IC_{50} values were calculated from isobolograms comparing cell proliferation as a percentage of RMS772 vector control cells (without inhibitor) and drug dose using CompuSyn (ComboSyn Incorporated).

Acknowledgments

The authors thank Bryan Clary for the pMSCVzeo retroviral luciferase gene construct and Kent Hunter (NCI) and Mauro Tiso (University of Pittsburgh, Pittsburgh, Pennsylvania, USA) for useful discussions. This work was supported in part by the Cooperative Human Tissue Network, which is funded by the NCI, and by the intramural programs of the NIH (NHLBI and NCI).

Received for publication April 29, 2009, and accepted in revised form August 5, 2009.

Address correspondence to: Javed Khan, Advanced Technology Center, 8717 Grovemont Circle, Bethesda, Maryland 20892-4605, USA. Phone: (301) 435-2937; Fax: (301) 480-0314; E-mail: khanjav@mail.nih.gov.

Stephen J. Qualman is deceased.

1. Parham, D.M., and Ellison, D.A. 2006. Rhabdomyosarcomas in adults and children: an update. *Arch. Pathol. Lab. Med.* **130**:1454–1465.
2. Raney, R.B., et al. 2001. Rhabdomyosarcoma and undifferentiated sarcoma in the first two decades of life: a selective review of intergroup rhabdomyosarcoma study group experience and rationale for Intergroup Rhabdomyosarcoma Study V. *J. Pediatr. Hematol. Oncol.* **23**:215–220.
3. Khan, J., et al. 2001. Classification and diagnostic prediction of cancers using gene expression profiling and artificial neural networks. *Nat. Med.* **7**:673–679.
4. Baird, K., et al. 2005. Gene expression profiling of human sarcomas: insights into sarcoma biology. *Cancer Res.* **65**:9226–9235.
5. Yu, Y., et al. 2004. Expression profiling identifies the cytoskeletal organizer ezrin and the developmental homeoprotein Six-1 as key metastatic regulators. *Nat. Med.* **10**:175–181.
6. Davicioni, E., et al. 2006. Identification of a PAX-FKHR gene expression signature that defines molecular classes and determines the prognosis of alveolar rhabdomyosarcomas. *Cancer Res.* **66**:6936–6946.
7. Lagha, M., et al. 2008. Pax3 regulation of FGF signaling affects the progression of embryonic progenitor cells into the myogenic program. *Genes Dev.* **22**:1828–1837.
8. Zhao, P., et al. 2006. Fgfr4 is required for effective muscle regeneration in vivo. Delineation of a MyoD-Tead2-Fgfr4 transcriptional pathway. *J. Biol. Chem.* **281**:429–438.
9. Zhao, P., and Hoffman, E.P. 2004. Embryonic myogenesis pathways in muscle regeneration. *Dev. Dyn.* **229**:380–392.
10. Eswarakumar, V.P., Lax, I., and Schlessinger, J. 2005. Cellular signaling by fibroblast growth factor receptors. *Cytokine Growth Factor Rev.* **16**:139–149.
11. Bellus, G.A., et al. 1995. A recurrent mutation in the tyrosine kinase domain of fibroblast growth factor receptor 3 causes hypochondroplasia. *Nat. Genet.* **10**:357–359.
12. Kan, S.H., et al. 2002. Genomic screening of fibroblast growth-factor receptor 2 reveals a wide spectrum of mutations in patients with syndromic craniosynostosis. *Am. J. Hum. Genet.* **70**:472–486.
13. Ding, L., et al. 2008. Somatic mutations affect key pathways in lung adenocarcinoma. *Nature.* **455**:1069–1075.
14. Rand, V., et al. 2005. Sequence survey of receptor tyrosine kinases reveals mutations in glioblastomas. *Proc. Natl. Acad. Sci. U. S. A.* **102**:14344–14349.
15. Pollock, P.M., et al. 2007. Frequent activating FGFR2 mutations in endometrial carcinomas parallel germline mutations associated with craniosynostosis and skeletal dysplasia syndromes. *Oncogene.* **26**:7158–7162.
16. Byron, S.A., et al. 2008. Inhibition of activated fibroblast growth factor receptor 2 in endometrial cancer cells induces cell death despite PTEN abrogation. *Cancer Res.* **68**:6902–6907.
17. Dutt, A., et al. 2008. Drug-sensitive FGFR2 mutations in endometrial carcinoma. *Proc. Natl. Acad. Sci. U. S. A.* **105**:8713–8717.
18. Greenman, C., et al. 2007. Patterns of somatic mutation in human cancer genomes. *Nature.* **446**:153–158.
19. Stephens, P., et al. 2005. A screen of the complete protein kinase gene family identifies diverse patterns of somatic mutations in human breast cancer. *Nat. Genet.* **37**:590–592.
20. Ezzat, S., Zheng, L., Zhu, X.F., Wu, G.E., and Asa, S.L. 2002. Targeted expression of a human pituitary tumor-derived isoform of FGF receptor-4 recapitulates pituitary tumorigenesis. *J. Clin. Invest.* **109**:69–78.
21. Sharp, R., et al. 2002. Synergism between INK4a/ARF inactivation and aberrant HGF/SF signaling in rhabdomyosarcomagenesis. *Nat. Med.* **8**:1276–1280.
22. Yue, P., and Moult, J. 2006. Identification and analysis of deleterious human SNPs. *J. Mol. Biol.* **356**:1263–1274.
23. Yue, P., Melamud, E., and Moult, J. 2006. SNPs3D: candidate gene and SNP selection for association studies. *BMC Bioinformatics.* **7**:166.
24. Sunyaev, S., et al. 2001. Prediction of deleterious human alleles. *Hum. Mol. Genet.* **10**:591–597.
25. Ramensky, V., Bork, P., and Sunyaev, S. 2002. Human non-synonymous SNPs: server and survey. *Nucleic Acids Res.* **30**:3894–3900.
26. Ng, P.C., and Henikoff, S. 2003. SIFT: Predicting amino acid changes that affect protein function. *Nucleic Acids Res.* **31**:3812–3814.
27. Chen, H., et al. 2007. A molecular brake in the kinase hinge region regulates the activity of receptor tyrosine kinases. *Mol. Cell.* **27**:717–730.
28. Lew, E.D., Bae, J.H., Rohmann, E., Wollnik, B., and Schlessinger, J. 2007. Structural basis for reduced FGFR2 activity in LADD syndrome: Implications for FGFR autoinhibition and activation. *Proc. Natl. Acad. Sci. U. S. A.* **104**:19802–19807.
29. Mohammadi, M., et al. 1998. Crystal structure of an angiogenesis inhibitor bound to the FGF receptor tyrosine kinase domain. *EMBO J.* **17**:5896–5904.
30. Torkamani, A., and Schork, N.J. 2008. Prediction of cancer driver mutations in protein kinases. *Cancer Res.* **68**:1675–1682.
31. Grand, E.K., Chase, A.J., Heath, C., Rahemtulla, A., and Cross, N.C. 2004. Targeting FGFR3 in multiple myeloma: inhibition of t(4;14)-positive cells by SU5402 and PD173074. *Leukemia.* **18**:962–966.
32. Marics, I., Padilla, F., Guillemot, J.F., Scaal, M., and Marcelle, C. 2002. FGFR4 signaling is a necessary step in limb muscle differentiation. *Development.* **129**:4559–4569.
33. Galili, N., et al. 1993. Fusion of a fork head domain gene to PAX3 in the solid tumour alveolar rhabdomyosarcoma. *Nat. Genet.* **5**:230–235.
34. Fredericks, W.J., et al. 1995. The PAX3-FKHR fusion protein created by the t(2;13) translocation in alveolar rhabdomyosarcomas is a more potent transcriptional activator than PAX3. *Mol. Cell. Biol.* **15**:1522–1535.
35. Sorensen, P.H., et al. 2002. PAX3-FKHR and PAX7-FKHR gene fusions are prognostic indicators in alveolar rhabdomyosarcoma: a report from the children's oncology group. *J. Clin. Oncol.* **20**:2672–2679.
36. Chen, Y., et al. 2008. Oncogenic mutations of ALK kinase in neuroblastoma. *Nature.* **455**:971–974.
37. George, R.E., et al. 2008. Activating mutations in ALK provide a therapeutic target in neuroblastoma. *Nature.* **455**:975–978.
38. Janoueix-Lerosey, I., et al. 2008. Somatic and germline activating mutations of the ALK kinase receptor in neuroblastoma. *Nature.* **455**:967–970.
39. Mosse, Y.P., et al. 2008. Identification of ALK as a major familial neuroblastoma predisposition gene. *Nature.* **455**:930–935.
40. Bromberg, J.F., et al. 1999. Stat3 as an oncogene. *Cell.* **98**:295–303.
41. Hart, K.C., et al. 2000. Transformation and Stat activation by derivatives of FGFR1, FGFR3, and FGFR4. *Oncogene.* **19**:3309–3320.
42. Chen, C.L., et al. 2007. Signal transducer and activator of transcription 3 is involved in cell growth and survival of human rhabdomyosarcoma and osteosarcoma cells. *BMC Cancer.* **7**:111.
43. Huang, S. 2007. Regulation of metastases by signal transducer and activator of transcription 3 signaling pathway: clinical implications. *Clin. Cancer Res.* **13**:1362–1366.
44. Yoeli-Lerner, M., et al. 2005. Akt blocks breast cancer cell motility and invasion through the transcription factor NFAT. *Mol. Cell.* **20**:539–550.
45. Liu, H., et al. 2006. Mechanism of Akt1 inhibition of breast cancer cell invasion reveals a protumorigenic role for TSC2. *Proc. Natl. Acad. Sci. U. S. A.* **103**:4134–4139.
46. Dufour, C., et al. 2008. FGFR2-Cbl interaction in lipid rafts triggers attenuation of PI3K/Akt signaling and osteoblast survival. *Bone.* **42**:1032–1039.
47. Demetri, G.D., et al. 2002. Efficacy and safety of imatinib mesylate in advanced gastrointestinal stromal tumors. *N. Engl. J. Med.* **347**:472–480.
48. Chen, Y., et al. 2006. Mutations of the PTPN11 and RAS genes in rhabdomyosarcoma and pediatric hematological malignancies. *Genes Chromosomes Cancer.* **45**:583–591.
49. Stratton, M.R., Fisher, C., Gusterson, B.A., and Cooper, C.S. 1989. Detection of point mutations in N-ras and K-ras genes of human embryonal rhabdomyosarcomas using oligonucleotide probes and the polymerase chain reaction. *Cancer Res.* **49**:6324–6327.
50. Yoo, J., and Robinson, R.A. 1999. H-ras and K-ras mutations in soft tissue sarcoma: comparative studies of sarcomas from Korean and American patients. *Cancer.* **86**:58–63.
51. Marks, J.L., et al. 2007. Mutational analysis of EGFR and related signaling pathway genes in lung Adenocarcinomas identifies a novel somatic kinase domain mutation in FGFR4. *PLoS ONE.* **2**:e426.
52. Wood, L.D., et al. 2007. The genomic landscapes of human breast and colorectal cancers. *Science.*

318:1108–1113.
53. Parsons, D.W., et al. 2008. An integrated genomic analysis of human glioblastoma multiforme. *Science.* **321**:1807–1812.
54. Jones, S., et al. 2008. Core signaling pathways in human pancreatic cancers revealed by global genomic analyses. *Science.* **321**:1801–1806.
55. Berndt, I., et al. 1998. A new hot spot for mutations in the ret protooncogene causing familial medullary thyroid carcinoma and multiple endocrine neoplasia type 2A. *J. Clin. Endocrinol. Metab.* **83**:770–774.
56. Bolino, A., et al. 1995. RET mutations in exons 13 and 14 of FMTC patients. *Oncogene.* **10**:2415–2419.
57. Wang, J.K., Gao, G., and Goldfarb, M. 1994. Fibroblast growth factor receptors have different signaling and mitogenic potentials. *Mol. Cell. Biol.* **14**:181–188.
58. Li, Z., et al. 2001. The myeloma-associated oncogene fibroblast growth factor receptor 3 is transforming in hematopoietic cells. *Blood.* **97**:2413–2419.
59. Bange, J., et al. 2002. Cancer progression and tumor cell motility are associated with the FGFR4 Arg(388) allele. *Cancer Res.* **62**:840–847.
60. Morimoto, Y., et al. 2003. Single nucleotide polymorphism in fibroblast growth factor receptor 4 at codon 388 is associated with prognosis in high-grade soft tissue sarcoma. *Cancer.* **98**:2245–2250.
61. Stadler, C.R., Knyazev, P., Bange, J., and Ullrich, A. 2006. FGFR4 GLY388 isotype suppresses motility of MDA-MB-231 breast cancer cells by EDG-2 gene repression. *Cell Signal.* **18**:783–794.
62. Barr, F.G., Xiong, Q.B., and Kelly, K. 1995. A consensus polymerase chain reaction-oligonucleotide hybridization approach for the detection of chromosomal translocations in pediatric bone and soft tissue sarcomas. *Am. J. Clin. Pathol.* **104**:627–633.
63. Stone, E.A., and Sidow, A. 2005. Physicochemical constraint violation by missense substitutions mediates impairment of protein function and disease severity. *Genome Res.* **15**:978–986.
64. Ngo, V.N., et al. 2006. A loss-of-function RNA interference screen for molecular targets in cancer. *Nature.* **441**:106–110.
65. Subramanian, A., et al. 2005. Gene set enrichment analysis: a knowledge-based approach for interpreting genome-wide expression profiles. *Proc. Natl. Acad. Sci. U. S. A.* **102**:15545–15550.
66. Khanna, C., et al. 2004. The membrane-cytoskeleton linker ezrin is necessary for osteosarcoma metastasis. *Nat. Med.* **10**:182–186.